Physics of multicellular systems

From cell to tissue mechanics

Hervé Turlier

February 13, 2023

Contents

Chapter 1

From cell to tissue tension

Multicellular aggregates generally adopt a spherical shape, which resembles the one of a liquid droplet. This suggests that tissues may have a surface tension. This idea was further developed by M. Steinberg in the 1960's [2].

1.1 Preliminaries [1]

1.1.1 Origin of liquid surface tension

Surface tension is, by definition, an energy per unit surface. Its unit is therefore $\mathrm{J.m^{-2}} = \mathrm{N.m^{-1}}$. In physics, it is commonly denoted by the symbol γ.

Surface tension is generally associated to liquid surfaces, and quantifies by essence, the fact that an interface between two immiscible phases costs an energy that is proportional to the interface area:

$$\delta\mathcal{E} = \gamma\delta A \tag{1.1}$$

At a given volume, the minimal surface of an isolated material is the sphere, which explains the spherical shape of droplets, bubbles etc...

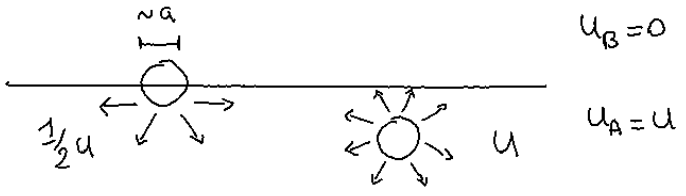

Figure 1.1: Origin of surface tension between a liquid and air.

Between two liquids A and B (or between a liquid A and a gaz B), a surface tension emerges from the different cohesion energies. In the limit of a gazeous phase B, we assume the cohesion energy U_B of molecules B to be zero., while the cohesion energy of molecules A is $U_\mathrm{A} = U > 0$. The following sketch shows graphically that surface tension is due to the loss of one half of the cohesion between A molecules at the interface between phases A and B.

If the size of the molecule A is a, the surface tension may be simply deduced as half of cohesion energy

divided by the typical surface a^2 of a molecule:

$$\gamma \sim \frac{1}{2}\frac{U}{a^2} \tag{1.2}$$

Examples of typical values of surface tension in the nature

- $\gamma_{\text{water}} \sim 72\text{mN.m}^{-1}$ for water/air interface at 25°C
- $\gamma_{\text{mercury}} \sim 486\text{mN.m}^{-1}$ for mercury/air interface at 25°C

1.1.2 Force balance: Laplace and Young-Dupré laws

Laplace's law
For an isolated droplet, there is only one relevant force balance equation, which is projected along the normal to the surface, and is named after Laplace. Laplace's law relates the difference of pressure between the inside and outside compartmentsP_{int} and P_{ext}, the surface tension γ and the curvature radius R by

$$\Delta P = P_{\text{int}} - P_{\text{ext}} = \frac{2\gamma}{R} \tag{1.3}$$

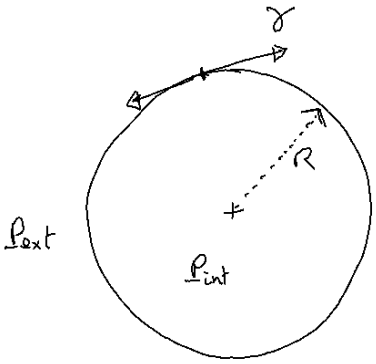

Figure 1.2: Laplace's law

The factor 2 stems from the fact that there are two principal curvature radii $R_1 = R_2 = R$, which are equivalent in a sphere. A generalized Laplace's formula for more complicated shapes and possibly for different tensions along the two principal curvature radii would read

$$P_{\text{int}} - P_{\text{ext}} = \frac{\gamma_1}{R_1} + \frac{\gamma_2}{R_2} \tag{1.4}$$

Wetting parameter and Young-Dupré's law
When a droplet enters in contact with a surface, it may adhere (generally partially) to it. One can define generically three surface tensions between the three phases (air, water, solid):

- $\gamma_{aw} = \gamma$ for the surface tension between air and water
- γ_{as} for the tension between air and solid
- γ_{sw} for the tension between the solid and water

The relevant parameter to measure the degree of droplet adhesion onto the surface (or spreading/weeting) is called a wetting (or spreading) parameter, defined as

$$S = \gamma_{as} - (\gamma_{sw} + \gamma) \tag{1.5}$$

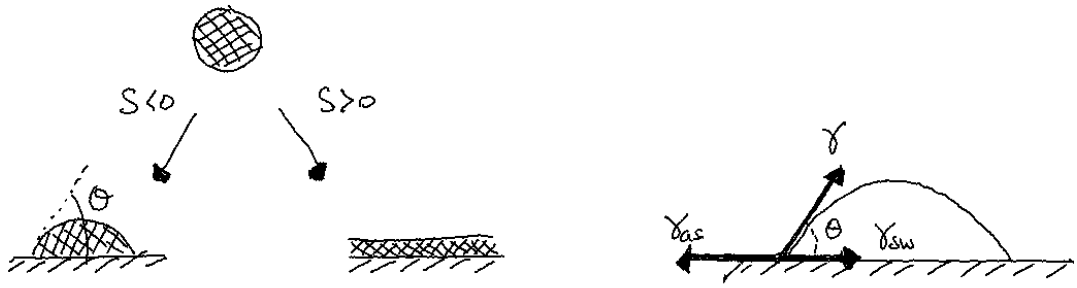

Figure 1.3: Total and partial wetting (left) and Young Dupré law (right)

- If $S > 0$ wetting is said to be total: the contact angle is zero and the droplet spreads onto the solid surface until forming a nanoscopic layer of fluid called precursor layer.
- If $S \leq 0$ wetting is partial, and the droplet contacts the solid substrate with an angle θ.

For partial wetting, the contact line follows Young-Dupré's tension balance, which may be expressed in a vectorial form:

$$\vec{\gamma} + \vec{\gamma_{sw}} + \vec{\gamma_{as}} = \vec{0} \tag{1.6}$$

or projecting onto the flat substrate, may also be expressed as function of the contact angle θ

$$\gamma \cos\theta = \gamma_{as} - \gamma_{sw} \tag{1.7}$$

1.2 Surface tension of a tissue

1.2.1 Steinberg's differential adhesion hypothesis

The differential adhesion hypothesis of Steinberg states that tissues have a tension (because they adopt spherical shapes in isolation) and that this tension is controlled by the cohesion (or adhesion) energy of cells within the tissue, in direct analogy with the physics of liquids.

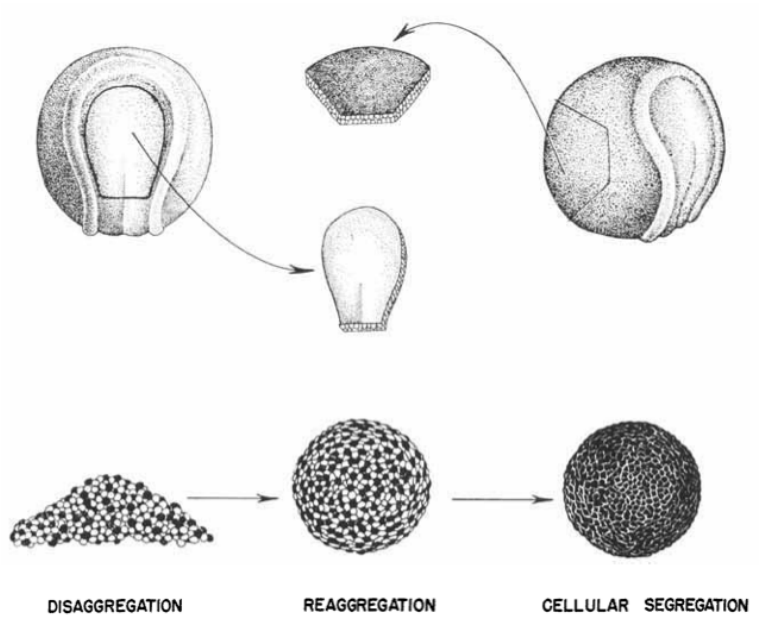

Figure 1.4: Sketch of the early experiments by Holtfreter [3]

This hypothesis was directly inspired by early experiments made by Holtfreter with fragments of amphibian embryos [3], where cells from endoderm and ectoderm precursor tissues were disagreggated and reaggregated. Forming a mixture, the resulting aggregate not only rounds up but the cells of different types also spontaneously sort out, with ectoderm cells at the exterior and endoderm cells in the interior, as naturally observed in the embryo (see Fig. 1.4). Later on, Steinberg performed a series of related experiments [2, 4] with various tissues to confirm that this behavior is generic and is directly correlated with a measurable tension of the tissue, and that such tissue tension is directly proportional to the amount of adhesion molecules between cells [5].

To quantitatively verify the differential adhesion hypothesis, Steinberg compares experiments with predicted configurations of minimal surface energy for a binary mixture of two liquids A and B,, characterized by homophilic cohesion energy densities w_A and w_B (between phases of same nature) and an heterophilic adhesion energy density w_{AB} (between phases of different nature) [2].

In general, one expects the free energy of the system to read

$$\mathcal{F} = -\int_{S_{AB}} w_{AB} dS - \int_{S_A} w_A dS - \int_{S_B} w_B dS \tag{1.8}$$

where S_{AB} is the area of heterophilic contacts between cells of types A and B, and S_A and S_B the area of contact between cells of same type, either A or B.

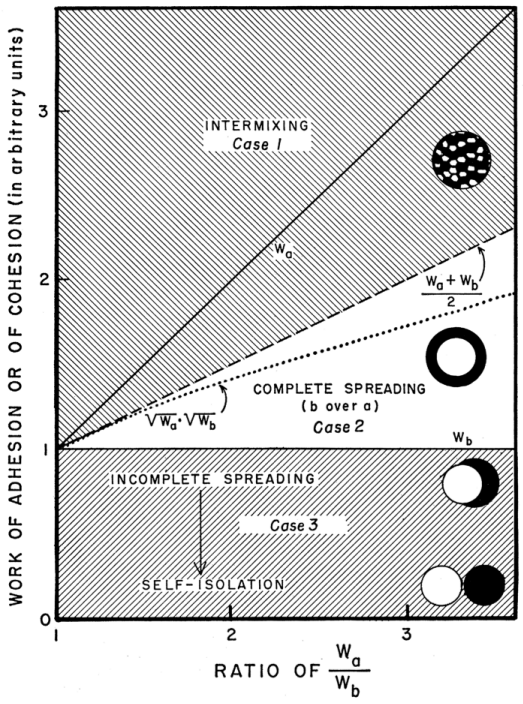

Figure 1.5: Phase diagram of the minimum energy configuration of binary mixture of cells of type A and B [2]

One may distinguish two main cases:

- If $w_{AB} \geq \frac{w_A + w_B}{2}$, one expects the energy to be minimum when the tissue forms a perfectly alternating mixture of cells A and B, which corresponds to the Case 1 in Fig. 1.5.
- If $w_{AB} < \frac{w_A + w_B}{2}$, one may expect, on the contrary, cells of type A and B to segregate in separated compartments. Several scenario are however possible in this case:
    1. If one supposes furtheremore that the adhesion strength between A and B cells is higher than between cells of type B themselves $w_{AB} \geq w_B$. This implies $\frac{w_A + w_B}{2} > w_{AB} \geq w_B$, which is possible only when $w_A > w_{AB} \geq w_B$. In such situation, where the cohesion strength of B is of

lesser extent, will tend to have it at the exterior, while A will tend to be inside the spherical aggregate, which corresponds to the complete spreading (Case 2 of Fig. 1.5).

2. If, on the contrary, one supposes $w_A \geq w_B > w_{AB}$, spreading is expected to be incomplete, corresponding to Case 3 on Fig. 1.5. In the limit of vanishing adhesion between A and B, one expects two separated isolated spherical aggregates.

1.2.2 Tension measurement

Parallel plates tensiometer

To quantitatively assess the predictions above, Steinberg and his collaborators have developed a tissue tensiometer based on the compression between two parallel plates [4, 6].

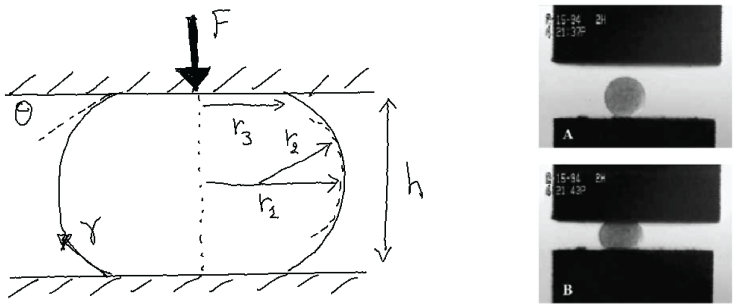

Figure 1.6: Parallel plate tensiometer

A compressive force F is applied by the upper plate on the tissue, that deforms and increases its pressure to resist the deformation and conserve its volume. The geometrical parameters describing the deformed tissue from a sphere are depicted on the Fig. 1.6.

Normal force balance on the contact surface between the cell aggregate and one plate reads

$$F + \gamma 2\pi r_3 \sin\theta = \Delta P \pi r_3^2 \tag{1.9}$$

In the midplane of the aggregate, where principal curvature radii are r_1 and r_2, Laplace's law reads furthermore $\Delta P = \gamma\left(\frac{1}{r_1} + \frac{1}{r_2}\right)$, leading to the following formula for the tissue tension

$$\gamma = \frac{F}{\pi r_3^2}\left(\frac{1}{r_1} + \frac{1}{r_2}\right)^{-1} \tag{1.10}$$

In [5, 6], geometric approximations are made, which consists in assuming circular arc shapes for the lateral tissue profile. If there is no adhesion between the tissue and the plate ($\theta = 0$), then $r_2 \sim \frac{2}{h}$ and $r_3 = r_1 - r_2$. If the tissue and the plate have a non-zero (partial) adhesion ($\frac{\pi}{2} > \theta > 0$), one may calculate r_3 from Pythagore theorem, yielding $r_3 = (r_1 - r_2) + \sqrt{r_2^2 - \left(\frac{h}{2}\right)^2}$. The optical determination of the contact angle θ is however generally tedious and imprecise.

In fact, the shape of lateral tissue profile shall not be circular, as the surface shall be of constant mean curvature following Laplace's law. The true profile is called an onduloid (or hyperbolic roulette), and the correct formula for the tension based on the exact solution of Laplace's equation was derived in [7].

Micropipette aspiration

An alternative technique to measure the surface tension of a liquid-like cell aggregate is the aspiration in a micropipette. The technique was developed by Mitchison and Swann in the 1950's to measure the surface tension of individual cells, and they called it *cell elastimeter* [8]. It consists in aspirating a portion of a

cell into a micropipette by applying a drop of pressure inside the pipette and to measure the length of the aspirated cap.

Following the original manuscript's notation (see Fig. 1.7, we define R the radius of the cell, d the diameter of the pipette, x the length of the aspirated length and r the curvature radius of the aspirated spherical cap.

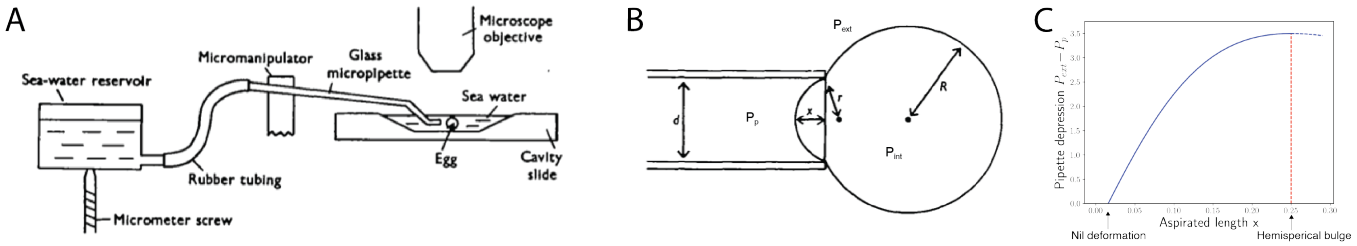

Figure 1.7: Micropipette aspiration: (**A**) General arrangement of *the cell elastimeter*. (**B**) Geometric parametrization of the problem. (**C**) Plot of the depression in the pipette as function of the aspirated cell cap length x [8].

Denoting γ the surface tension of the cell, P_{int} the pressure inside the cell, P_{ext} the pressure of the external medium, and P_{p} the pressure inside the pipette, we may write Laplace's law at the interface between the cell and the external medium $P_{\text{int}} - P_{\text{ext}} = 2\gamma/R$ and between the cell and the pipette $P_{\text{int}} - P_{\text{p}} = 2\gamma/r$. Combining the two equations we obtain the pressure drop in the pipette as function of the cell geometry $P_{\text{ext}} - P_{\text{p}} = 2\gamma\left(\frac{1}{r} - \frac{1}{R}\right)$.

Using Pythagore theorem, we furthermore have $r^2 = (d/2)^2 + (r-x)^2$, such that

$$P_{\text{ext}} - P_{\text{p}} = 2\gamma\left(\frac{2x}{x^2 + d^2/4} - \frac{1}{R}\right) \tag{1.11}$$

The pressure drop in the pipette may be plotted as function of x as shown on Fig.1.7C, assuming that R remains approximately constant (small pipette). The tension may be deduced by fitting the linear part of this curve

In the limit case, where $x \sim r \sim d/2$ (which is often used experimentally, although the cell configuration becomes metastable), one gets simply $P_{\text{ext}} - P_{\text{p}} \sim 2\gamma\left(\frac{2}{d} - \frac{1}{R}\right) \equiv \Delta P_c$, where ΔP_c is often called "critical" pressure. Above the critical pressure, the cell will as the pressure difference in the pipette decreases with the length of the aspirated cell portion.

This technique was recently applied ti spherical cell aggregates by Guevorkian et al. [9]. The tension value they measured is $\gamma \approx 6\text{mN.m}^{-1}$ for murin sarcoma cells (S180). In this study, they did not only measure the tension of the tissue but by measuring the speed of the entry of the cell tongue inside the micropipette, they could also extract viscoelastic parameters characterizing the aggregate.

Magnetic tensiometer

Recently, an original method [10] was developed to measure the tension of a tissue by a method mimicking the so-called sessile drop tension measurement (see Fig. 1.8). A sessile drop is of radius larger than the capillary size[1] $\kappa^{-1} \sim \sqrt{\frac{\gamma}{\rho g}}$, and will be flattened by gravity. The profile of the drop results from the competition between gravity and surface tension forces, and its fitting may allow to come back to a numerical evaluation of the fluid surface tension. However, for tissues, this capillary size is of the order of $\sim \sqrt{\frac{10^{-2}}{10^3 \times 10}} = 1\,\text{mm}$, while typical cell aggregates generated *in silico* are generally also of maximum size $100\,\mu\text{m} - 1\text{mm}$ which does not lead to large deformations allowing for direct application of the sessile drop method. Therefore, the

[1]The capillary size compares the Laplace's pressure created by the surface tension $\sim \gamma/\kappa^{-1}$ and the hydrostatic pressure created by gravity $\sim \rho g \kappa^{-1}$ (with ρ the fluid density and g the gravitational field strength on Earth).

authors have got the idea to incorporate ferromagnetic nanoparticles into cells, and to generate a magnetic field gradient to create a bulk magnetic force in cells along the vertical direction of magnitudes up to $\sim 150\,\mathrm{g}$. The typical magnetic force per unit volume they generate is $\vec{f_v} = \nabla\left(\vec{M}_v \cdot \vec{B}\right) \sim 10^5 \mathrm{N.m}^{-3}$, and they measure typical tissue surface tensions $\gamma \sim 10\,\mathrm{mN.m}^{-1}$ [10, 11].

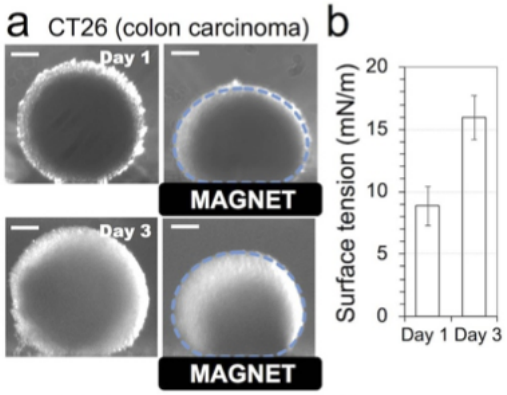

Figure 1.8: Magnetic tensionmeter: (**a**) Profiles of cell aggregates before and after application of the magnetic field gradient. (**b**) Typical values of tensions measured after 1 and 3 days [11].

1.3 Origin of tissue tension

1.3.1 Differential Adhesion vs Tension Hypothesis

After the initial differential adhesion hypothesis (DAH) of Steinberg [2], a long physical debate has animated the community about the true physical origin of the surface tension in a tissue. One of the first author to openly criticize Steinberg's hypothesis is Albert K. Harris in a long discussion [12], where alternative explanations for the emergence of a tissue tension are proposed. In contrast to the assumption that cells would behave exactly like molecules in a fluid, Harris promotes the notion of differential contraction (or differential contractility hypothesis DCH) as the most likely explanation of tissue sorting phenomena. His idea is based on the fact that cells are known to have a contractile surface that generates also a surface tension at the cell level, that may be controlled by several cellular processes,. In particular, contractility may be reduced at cell-cell interfaces but may also depend on the cell type. In this scenario, the rounding up of aggregates may be explained by the formation of a (more) contractile layer composed of the exposed portions of cells located at the aggregate surface. The contraction of this surface layer would minimize the exposed surface area and round up the aggregate. Similarly, the engulfment of one aggregate into another may be explained by a diffential of contractility between them, where the more contractile aggregate will gradually pull the other aggregate around it. One difficulty that Harris raises is the difficulty to differentiate the DAH from the DCH, although he predicts that inhibiting contractility by drugs depolymerizing the cortical layer could lead to large decrease in tissue tension, that could not be explained by the DAH.

First numerical simulations of cell sorting used were realized by Graner and Glazier using Potts models [13] (Monte Carlo simulations on a fixed grid) and could realistically simulate the process of sorting starting from an initial configuration with randomly assigned cell types (see Fig. 1.9A).

More recently, G. Wayne Brodland proposed to replace the concept of DAH or DCH by the concept of differential interfacial tension hypothesis (DITH), which may encompass both effects of adhesion energy and contractile tension by defining cells configuration through the balance of interfacial tensions [14]. Performing 2D simulations using finite elements, Brodland could reproduce and characterize many of the observations of partial and total engulfment observed in 3D tissues (see Fig. 1.9B).

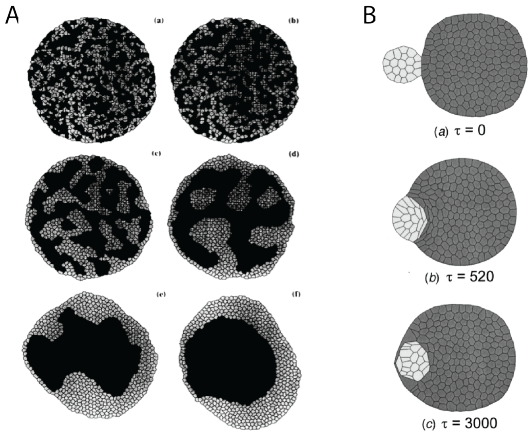

Figure 1.9: Simulations of sorting: (A) Potts simulations of cell sorting [13]. (B) Finite-element simulations of tissue engulfment [14].

1.3.2 Cortical tension and adhesion coupling

The fact that cells in suspension are round is a strong sign of a surface tension. But where is this tension coming from? The surface of cells is composed of plasma membrane (lipid bilayer), which separates topologically the cell interior and exterior, to which is attached a cortical layer made of a thin network of semi-flexible polymer filaments (a few 100nm thick). These filaments called actin are under fast renewal (about 30s to 1min turnover time), are crosslinked by various proteins (α-actinin, plastin, fascin, filamin, Arp2/3...) and put under tension by minifilaments of molecular motors called myosins (see Fig. 1.10A). The activity of molecular motors creates a contractile stress in this gel, that results into an effective surface tension called cortical tension. The tension $\gamma_{\rm cell}$ at the surface of a cell is therefore generically the result of two contributions a cortical tension $\gamma_{\rm cortex} \sim 100{\rm pN}/\mu{\rm m}$ and a membrane tension $\gamma_{\rm membrane} \sim 10{\rm pN}/\mu{\rm m}$. The latter is generally an order of magnitude lower than the cortical tension, such that most of the tension at the cell surface may be attributed to the cortical contractility.

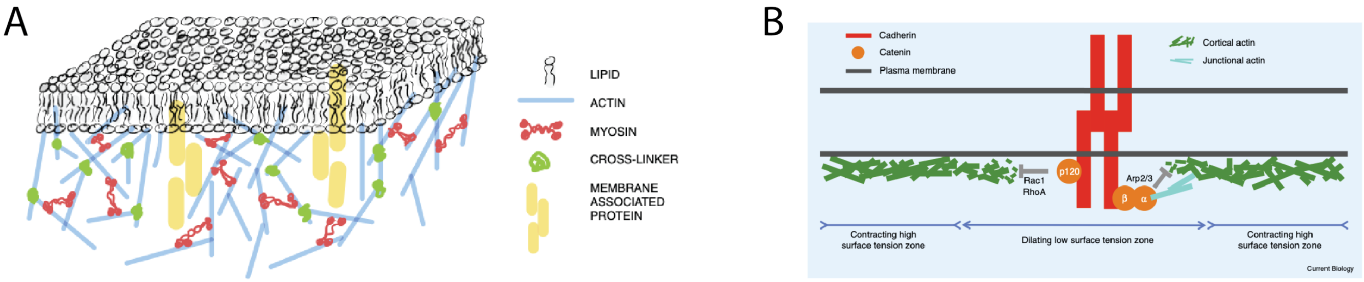

Figure 1.10: (A) Sketch of the cell surface with the lipid bilayer and cortical components [15]. (B) Sketch of the negative feedback mechanism of cell adhesion through cadherins onto the cell cortex [16].

The recent experiments in the field confirm Harris's hypothesis that contractility is the main origin of tissue tension and that sorting phenomena relies on differential interfacial tension [17]. The main idea is that adhesion couples mechanically cell surfaces and decreases contractility at interfaces through negative signaling feedback from bound cadherin adhesion molecules to the cortex (see Fig. 1.10B).

Yet there is still no complete generic consensus on the absolute contribution of the adhesion energy [16]. Generically, defining the tension $\gamma_{\rm cm}$ at a free interface in contact with the cell medium, one may define the tension at a cell-cell contact $\gamma_{\rm cc} \sim 2\beta\gamma_{\rm cm} - W$, where W is the direct negative energetic contribution arising by the binding of adhesion molecules and β measures the degree of cortical depletion at cell-cell interfaces.

From the knowledge of the tensions $\gamma_{\rm cmi}$ and $\gamma_{\rm cc}$, one can generically predict the configuration of a cell doublet.

1.3.3 L. Manning's model of tissue tension

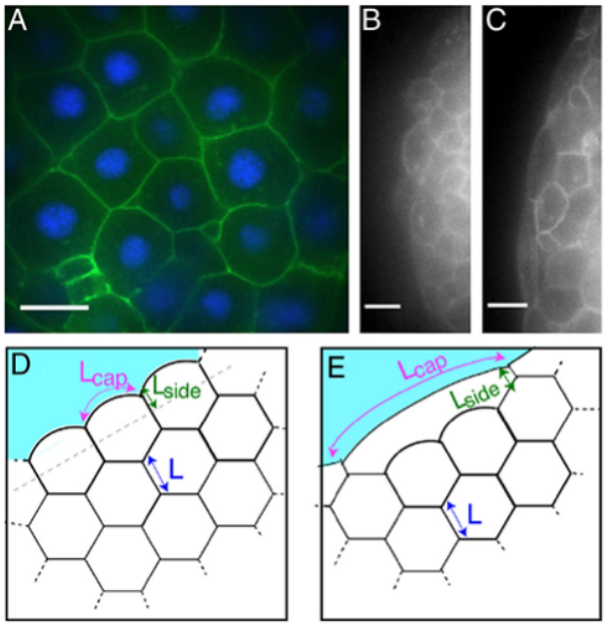

Figure 1.11: (A) Confocal section of a zebrafish aggregate. (B) Surface cells where E-cadherin is down-regulated. (C) Surface cells of an ectoderm aggregate. (C) and (D) Corresponding schematics of cell arrangement and shape.: cells at the surface maintain a compact shape (C) or spread on their underlying neighbors (n=3) [18].

Lisa Manning is one the first to have proposed a quantitative analytic model to evaluate the tension of a tissue as function of the cortical tension and adhesion of individual cells. The model is in 2D, but should qualitatively hold in 3D. The Fig. 1.11A shows a section of cells close to the surface of an aggregate of zebrafish embryo cells, showing an approximate hexagonal organization. Manning therefore assumes this organization for the whole tissue, with however two different cases for cells at the surface, the interface of which with the cell medium shall round up because of Laplace's pressure. Two cases are observed experimentally:

(a) When the expression of the E-cadherin adhesion molecule is down-regulated, the embryo surface displays compact cells, which do not elongate over the aggregate surface.

(b) When the aggregate is formed with ectoderm embryonic cells, surface cells tend to elongate to spread over $n \sim 3$ underlying neighbors.

Below we will follow the calculation of tissue tension made by Manning in 2D for these two cases.

(a) Compact surface cells

Calling γ_i the line tension of each cell edge i, the total energy of the tissue is

$$\mathcal{E} = \sum_{i\,\text{in}} 2\Gamma_i L_i + \sum_{i\,\text{surf}} \gamma_i \ell_i \tag{1.12}$$

There are two types of interfaces. The interfaces between two cells for which $\Gamma_i = \Gamma_0 = \Gamma_a - \frac{W}{2}$, where Γ_a is the active tension of the cortex at cell-cell interfaces and W the adhesion energy per unit line. The cell-medium interfaces may have a different contractility and have no adhesion contribution, they are denoted by $\gamma_i = \gamma_s$. Cells are supposed to have a constant area. Because of this constraint surface cells are deformed $\tilde{L} \neq L$ and this deformation contributes to the tissue surface tension. In the next we introduced an effective adhesion energy $\omega = W + 2(\gamma_s - \Gamma_a)$, which includes the real adhesion and the difference of cortical tensions between the inside and surface of the tissue.

The energy of one cell inside the tissue becomes

$$\epsilon_{\text{in}} = 6L\left(\Gamma_a - \frac{W}{2}\right) = 6L\left(\gamma_s - \frac{\omega}{2}\right) \tag{1.13}$$

and for a cell at the tissue surface

$$\epsilon_{\text{surf}} = 2\left(L + \tilde{L}\right)\left(\gamma_s - \frac{\omega}{2}\right) + \ell\gamma_s \tag{1.14}$$

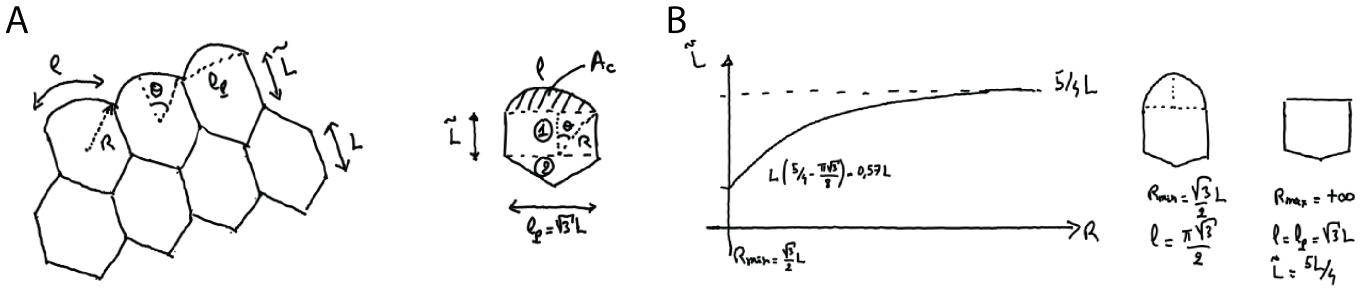

Figure 1.12: (A) Geometrical parametrization of the compact tissue configuration. (B) Plot of $\tilde{L}$ as function the curvature radius R of outer interfaces.

The tissue (line) tension may then be defined as the difference of energy between a cell at the surface and inside the tissue, divided by the length of a cell at the surface $\ell_p = 2L\sin 2\pi/3 = \sqrt{3}L$

$$\sigma \equiv \left(\frac{\Delta\mathcal{E}}{\text{one cell}}\right)\left(\frac{\text{one cell}}{A_{\text{proj}}}\right) = \frac{\epsilon_{\text{surf}} - \epsilon_{\text{in}}}{\ell_p} = \frac{\ell\gamma_s + \left(\gamma_s - \frac{\omega}{2}\right)\left(2\tilde{L} - 4L\right)}{\sqrt{3}L} \tag{1.15}$$

Now we can use the area constraint to calculate the relation between the curvature radius of the curved edge at the border, and the lateral length of surface cells: $A = 6\frac{L\sqrt{3}}{2}\frac{L}{2} = \frac{3\sqrt{3}}{2}L^2 = A_c + A_1 + A_2$.

We have furthermore $A_1 = \tilde{L}\,\ell_p = \sqrt{3}L\tilde{L}$, $A_2 = \frac{\sqrt{3}}{4}L^2$ and $A_c = R^2\theta - \frac{\ell_p}{2}R\cos\theta = R^2\theta - \frac{\sqrt{3}}{2}RL\cos\theta$, which leads to the relation

$$\tilde{L} = \frac{5}{4}L - \frac{A_c}{L\sqrt{3}} \tag{1.16}$$

and we can plot $\tilde{L}$ as function of R as shown on Fig. 1.12

There are two limit cases:

- When the upper portion of surface cells makes an hemisphere $R = R_{\min} = \frac{\sqrt{3}}{2}L$, then $\tilde{L} = L\left(\frac{5}{4} - \frac{\pi\sqrt{3}}{8}\right)$ and $\ell = \frac{\pi\sqrt{3}}{2}$. The tissue tension becomes $\sigma = \frac{\pi}{2}\gamma_s - \left(\gamma_s - \frac{\omega}{2}\right)1.64$
- When the upper portion of surface cells is flat $R = R_{\max} = +\infty$, then $\ell = \ell_p = \sqrt{3}L$ and $\tilde{L} = \frac{5}{4}L$. The tissue tension becomes $\sigma = \gamma_s - \frac{\sqrt{3}}{2}\left(\gamma_s - \frac{\omega}{2}\right) \geq 0$.

For a given fixed value of $\frac{\omega}{\gamma_s}$, the $\tilde{L}$ will be the one that minimizes the surface energy (force balance). Manning has solved numerically this equation and can hence calculate the surface tension for any value of the ratio $\frac{\omega}{\gamma_s}$, as shown on Fig. 1.13.

If $\frac{\omega}{\gamma_s} \geq 2$, the effective adhesion energy dominates over the tension at the surface and surface cells will spread over more than a single inside cell. This is the case discussed below in the paragraph **(b)**. If $\frac{\omega}{\gamma_s}$ becomes too small, then the tissue surface tension becomes negative. The value $\sigma = 0$ is obtained for $R = R_{\min}$ and $\frac{\omega}{\gamma_s} = 0.186$. Below this value the tissue is not confluent anymore (not fully compacted).

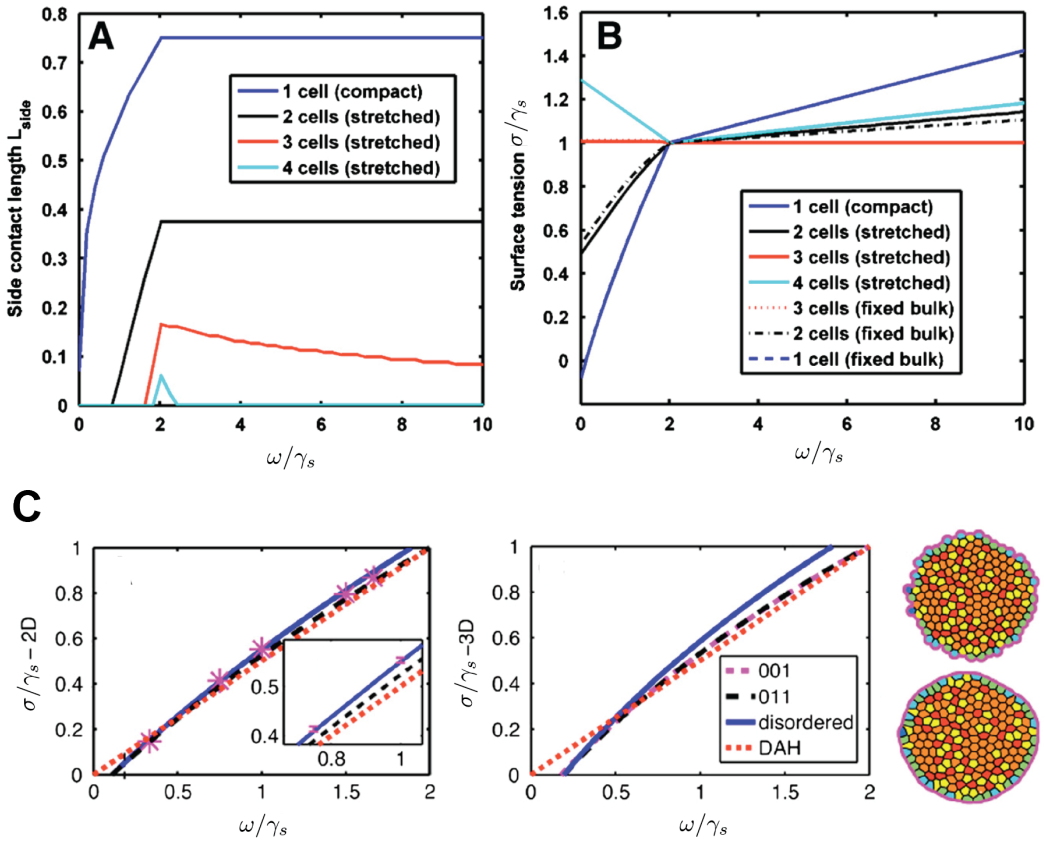

Figure 1.13: (A) Contact length $\tilde{L}$ of surface cells as function of the ratio of adhesion and surface cortical tension ω/γ_s (B) Plot of the normalized tissue tension σ/γ_s as function the curvature radius R of outer interfaces. (C) Plot of the tissue surface tension σ in units γ_s as function of ω/γ_s. The dashed black line is the analytic calculation for ordered packing, the blue line for a disordered aggregate. The dotted red line is $\sigma = \omega/2$ corresponding to the DAH. On the right are examples of minimum energy aggregate simulations in 2D for $\omega/\gamma_s \sim 0.33$ and $\omega/\gamma_s \sim 1.667$ [18]

(b) Elongated surface cells

For strong adhesion $\frac{\omega}{\gamma_s} \geq 2$, the surface cells will spread over several underlying cells from the previous layer. The tissue surface tension becomes simply γ_s and a surface cell will elongate as much as possible to minimize area. A regulation mechanism is then necessary to limit spreading, for example the availability of cadherin molecules. In her work, Manning introduces in 2D a term proportional to the squared perimeter for each cell, that limits the spreading. There could also be deformations of internal cells as a response to surface cells spreading, but numerical simulations predict that they remain very small and may therefore not contribute much to tissue tension.

Conclusion

Generalizing her results to 3 dimensions using numerical simulations, L. Manning obtains qualitatively similar results and she finds (see Fig. 1.13C) that Steinberg's hypothesis is relatively well verified theoretically for $\omega < 2\gamma_s$ (with an effective adhesion strength ω per unit surface instead of the pure adhesion energy W). At stronger adhesion strengths, the tissue surface tension $\sigma \sim \gamma_s$ and surface cells become much more elongated.

Bibliography

[1] Pierre-Gilles De Gennes, Françoise Brochard-Wyart, David Quéré, et al. *Capillarity and wetting phenomena: drops, bubbles, pearls, waves*, volume 336. Springer, 2004.

[2] Malcolm S Steinberg. Reconstruction of tissues by dissociated cells. *Science*, 141(3579):401–408, 1963.

[3] Philip L Townes and Johannes Holtfreter. Directed movements and selective adhesion of embryonic amphibian cells. *Journal of experimental zoology*, 128(1):53–120, 1955.

[4] Ramsey A Foty, Cathie M Pfleger, Gabor Forgacs, and Malcolm S Steinberg. Surface tensions of embryonic tissues predict their mutual envelopment behavior. *Development*, 122(5):1611–1620, 1996.

[5] Ramsey A Foty and Malcolm S Steinberg. The differential adhesion hypothesis: a direct evaluation. *Developmental biology*, 278(1):255–263, 2005.

[6] Ramsey A Foty, Gabor Forgacs, Cathie M Pfleger, and Malcolm S Steinberg. Liquid properties of embryonic tissues: measurement of interfacial tensions. *Physical review letters*, 72(14):2298, 1994.

[7] C Norotte, F Marga, A Neagu, I Kosztin, and G Forgacs. Experimental evaluation of apparent tissue surface tension based on the exact solution of the Laplace equation. *European Physical Letters*, 81(4): 46003, January 2008.

[8] JMt Mitchison and MM Swann. The mechanical properties of the cell surface. *J. exp. Biol*, 31(3): 443–460, 1954.

[9] Karine Guevorkian, Marie-Josée Colbert, Mélanie Durth, Sylvie Dufour, and Françoise Brochard-Wyart. Aspiration of biological viscoelastic drops. *Physical review letters*, 104(21):218101, 2010.

[10] Francois Mazuel, Myriam Reffay, Vicard Du, Jean-Claude Bacri, Jean-Paul Rieu, and Claire Wilhelm. Magnetic flattening of stem-cell spheroids indicates a size-dependent elastocapillary transition. *Physical review letters*, 114(9):098105, 2015.

[11] Jose E Perez, Irène Nagle, and Claire Wilhelm. Magnetic molding of tumor spheroids: emerging model for cancer screening. *Biofabrication*, 13(1):015018, 2020.

[12] Albert K Harris. Is cell sorting caused by differences in the work of intercellular adhesion? a critique of the steinberg hypothesis. *Journal of theoretical biology*, 61(2):267–285, 1976.

[13] François Graner and James A Glazier. Simulation of biological cell sorting using a two-dimensional extended potts model. *Physical review letters*, 69(13):2013, 1992.

[14] G Wayne Brodland. The differential interfacial tension hypothesis (dith): a comprehensive theory for the self-rearrangement of embryonic cells and tissues. *J. Biomech. Eng.*, 124(2):188–197, 2002.

[15] K Vijay Kumar. The actomyosin cortex of cells: A thin film of active matter. *Journal of the Indian Institute of Science*, 101(1):97–112, 2021.

[16] Jean-Léon Maître and Carl-Philipp Heisenberg. Three functions of cadherins in cell adhesion. *Current Biology*, 23(14):R626–R633, 2013.

[17] Jean-Léon Maître, Hélène Berthoumieux, Simon Frederik Gabriel Krens, Guillaume Salbreux, Frank Jülicher, Ewa Paluch, and Carl-Philipp Heisenberg. Adhesion functions in cell sorting by mechanically coupling the cortices of adhering cells. *science*, 338(6104):253–256, 2012.

[18] M Lisa Manning, Ramsey A Foty, Malcolm S Steinberg, and Eva-Maria Schoetz. Coaction of intercellular adhesion and cortical tension specifies tissue surface tension. *Proceedings of the National Academy of Sciences*, 107(28):12517–12522, 2010.

[19] Andrew R Harris, Loic Peter, Julien Bellis, Buzz Baum, Alexandre J Kabla, and Guillaume T Charras. Characterizing the mechanics of cultured cell monolayers. *Proceedings of the National Academy of Sciences*, 109(41):16449–16454, 2012.

[20] Matthias Merkel, Raphaël Etournay, Marko Popović, Guillaume Salbreux, Suzanne Eaton, and Frank Jülicher. Triangles bridge the scales: Quantifying cellular contributions to tissue deformation. *Physical Review E*, 95(3):032401, 2017.

[21] S Ishihara, K Sugimura, SJ Cox, Isabelle Bonnet, Y Bellaïche, and F Graner. Comparative study of non-invasive force and stress inference methods in tissue. *The European Physical Journal E*, 36(4):1–13, 2013.

[22] Reza Farhadifar, Jens-Christian Röper, Benoit Aigouy, Suzanne Eaton, and Frank Jülicher. The influence of cell mechanics, cell-cell interactions, and proliferation on epithelial packing. *Current Biology*, 17(24):2095–2104, 2007.

[23] Douglas B Staple, Reza Farhadifar, J-C Röper, Benoit Aigouy, Suzanne Eaton, and Frank Jülicher. Mechanics and remodelling of cell packings in epithelia. *The European Physical Journal E*, 33(2): 117–127, 2010.

[24] Edouard Hannezo, Jacques Prost, and Jean-Francois Joanny. Theory of epithelial sheet morphology in three dimensions. *Proceedings of the National Academy of Sciences*, 111(1):27–32, 2014.

[25] Hisao Honda, Masaharu Tanemura, and Tatsuzo Nagai. A three-dimensional vertex dynamics cell model of space-filling polyhedra simulating cell behavior in a cell aggregate. *Journal of theoretical biology*, 226 (4):439–453, 2004.

[26] Satoru Okuda, Takashi Miura, Yasuhiro Inoue, Taiji Adachi, and Mototsugu Eiraku. Combining turing and 3d vertex models reproduces autonomous multicellular morphogenesis with undulation, tubulation, and branching. *Scientific reports*, 8(1):1–15, 2018.

[27] Jean-Léon Maître, Hervé Turlier, Rukshala Illukkumbura, Björn Eismann, Ritsuya Niwayama, François Nédélec, and Takashi Hiiragi. Asymmetric division of contractile domains couples cell positioning and fate specification. *Nature*, 536(7616):344–348, 2016.

[28] Jorge Nocedal and Stephen J Wright. Conjugate gradient methods. *Numerical optimization*, pages 101–134, 2006.

[29] Sybren Ruurds De Groot and Peter Mazur. *Non-equilibrium thermodynamics*. Courier Corporation, 2013.

[30] Karsten Kruse, Jean-Francois Joanny, Frank Jülicher, Jacques Prost, and Ken Sekimoto. Generic theory of active polar gels: a paradigm for cytoskeletal dynamics. *The European Physical Journal E*, 16(1): 5–16, 2005.

[31] Paul M Chaikin, Tom C Lubensky, and Thomas A Witten. *Principles of condensed matter physics*, volume 10. Cambridge university press Cambridge, 1995.

[32] Vikram Deshpande, Antonio DeSimone, Robert McMeeking, and Pierre Recho. Chemo-mechanical model of a cell as a stochastic active gel. *Journal of the Mechanics and Physics of Solids*, 151:104381, 2021.

[33] P Yo Chou. On velocity correlations and the solutions of the equations of turbulent fluctuation. *Quarterly of applied mathematics*, 3(1):38–54, 1945.

[34] Pierre-Gilles De Gennes and Jacques Prost. *The physics of liquid crystals*. Number 83. Oxford university press, 1993.

[35] S Fürthauer, M Strempel, Stephan W Grill, and Frank Jülicher. Active chiral fluids. *The European physical journal E*, 35(9):1–13, 2012.

[36] G Duclos, C Blanch-Mercader, V Yashunsky, G Salbreux, J-F Joanny, J Prost, and Pascal Silberzan. Spontaneous shear flow in confined cellular nematics. *Nature physics*, 14(7):728–732, 2018.

[37] Guillaume Duclos, Christoph Erlenkämper, Jean-François Joanny, and Pascal Silberzan. Topological defects in confined populations of spindle-shaped cells. *Nature Physics*, 13(1):58–62, 2017.

[38] Morgan Delarue, Fabien Montel, Danijela Vignjevic, Jacques Prost, Jean-François Joanny, and Giovanni Cappello. Compressive stress inhibits proliferation in tumor spheroids through a volume limitation. *Biophysical journal*, 107(8):1821–1828, 2014.

[39] Fabien Montel, Morgan Delarue, Jens Elgeti, Laurent Malaquin, Markus Basan, Thomas Risler, Bernard Cabane, Danijela Vignjevic, Jacques Prost, Giovanni Cappello, et al. Stress clamp experiments on multicellular tumor spheroids. *Physical review letters*, 107(18):188102, 2011.

[40] Morgan Delarue, Fabien Montel, Ouriel Caen, Jens Elgeti, Jean-Michel Siaugue, Danijela Vignjevic, Jacques Prost, Jean-François Joanny, and Giovanni Cappello. Mechanical control of cell flow in multicellular spheroids. *Physical review letters*, 110(13):138103, 2013.

[41] Jonas Ranft, Markus Basan, Jens Elgeti, Jean-François Joanny, Jacques Prost, and Frank Jülicher. Fluidization of tissues by cell division and apoptosis. *Proceedings of the National Academy of Sciences*, 107(49):20863–20868, 2010.